J Nanostruct 11(2): 377-387, Spring 2021

RESEARCH PAPER

$Gd_{0.745}Y_{1.255}O_3$ and $Yb_{1.4}Y_{0.6}O_3$ Mixed Rare-earth-yttrium Oxides Nano-powders: Synthesis, Characterization, Particle-size Distribution and Optical Properties

*Dalila Mouattah [1,2] *, Soraya Belhadj [1,3], Mohamed Benabdallah Taouti [1,3] , and Djamel Benbertal [1,2]*

[1] *Laboratory Physico- Chemistry of Materials (LPCM), University of Amar Telidji, Laghouat, Algeria*

[2] *Department of Material Science, Faculty of Sciences, University of Amar Telidji, Laghouat, Algeria*

[3] *Department of Process Engineering, Faculty of Technology, University of Amar Telidji, Laghouat, Algeria*

ARTICLE INFO

Article History:
Received 14 November 2020
Accepted 15 March 2021
Published 01 April 2021

Keywords:
Co-precipitation synthesis
DRX
Mixed rare earth-yttrium oxides
Nano-powders; Optical properties
Yttrium oxide ceramics

ABSTRACT

$Gd_{0.745}Y_{1.255}O_3$ and $Yb_{1.4}Y_{0.6}O_3$ nano-powders of mixed rare-earth-yttrium sesquioxides (diluted magnetics) were successfully synthesized via a simple co-precipitation method using rare-earth-nitrate salts as cation precursors and followed by a 4 hour heat-treatment at various temperatures (600 °C, 800 °C and 1000°C) for material crystallization. Experiments demonstrated the role of pH on the "co-precipitation" synthesis of $Gd_{0.745}Y_{1.255}O_3$ and $Yb_{1.4}Y_{0.6}O_3$ nano-powders. The pH values were adjusted by adding NaOH which, as a precipitating agent, has a key role in this process. The obtained nano-powders were characterized by X-ray powder diffraction; their morphologies were analyzed by scanning electron microscope SEM, their average sizes were calculated using Scherrer formula, and their optical properties were studied using UV-Vis spectrophotometer with Tauc plot estimation to determine the band-gap energy. The influence of heat treatment, on the morphology and crystallite sizes of $Gd_{0.745}Y_{1.255}O_3$ and $Yb_{1.4}Y_{0.6}O_3$ nano-powders, was studied. The results indicated that the agglomeration of particles was favored by hydroxide precipitation, one of many other factors, including temperature and calcination time, that influence the quality of $Gd_{0.745}Y_{1.255}O_3$ and $Yb_{1.4}Y_{0.6}O_3$ nano-powders according to the SEM images, while the XRD analysis showed that crystallinity increased with an increase in calcination temperature. The study of particle-size distribution at different calcination temperatures indicated that the Grain-size increased from ~42 nm to ~100 nm for $Gd_{0.745}Y_{1.255}O_3$ and from ~13 nm to ~50 nm for $Yb_{1.4}Y_{0.6}O_3$ as the calcination temperatures increased, this influence also the optical band-gap which found to be decreasing from 4.22 to 3.95 eV when the particle sizes increasing for $Yb_{1.4}Y_{0.6}O_3$.

How to cite this article
Mouattah D, Belhadj S, Benabdallah Taouti M, Benbertal D. $Gd_{0.745}Y_{1.255}O_3$ and $Yb_{1.4}Y_{0.6}O_3$ Mixed Rare-earth-yttrium Oxides Nano-powders: Synthesis, Characterization, Particle-size Distribution and Optical Properties. J Nanostruct, 2021; 11(2):377-387. DOI: 10.22052/JNS.2021.02.017

INTRODUCTION

Recently, many researches have been conducted on improving the quality and use of materials for meeting the new requirement. Oxide Ceramics are extraordinary materials (especially non-Centrosymmetric ones) that are exploited in

* *Corresponding Author Email: d.mouattah@lagh-univ.dz*

many scientific and industrial fields such as signal processing (electronics, telecommunications, etc.) where electrochemical impedances and electrical resonance phenomena commonly used in many technologies [1-4], and in sensors and actuators field [5-10] (by capturing or transforming physical quantities) where piezoelectric materials have been increasingly used. In addition, nano-crystalline ceramic-oxides have been also studied for their quantum size effects [11-15].

Our particular interest to study the ABO_3 ceramic materials is raised in the contentious literature [16-20]. For example, Sr-doped $LaYO_3$ has been introduced as potential anode materials for solid oxide fuel cells [21,22]. These materials have catalytic properties, especially the perovskite-type oxides [23-28], which are also known to show an excellent proton conductivity at intermediate temperatures [29,30].

Both $GdYO_3$ and $YbYO_3$ have high thermal and chemical stability and high luminescence efficiency [31]. As a very good luminescent material, the mixed oxide $GdYO_3$ ceramic doped with Eu^{3+} ions has been used to provide red light emissions in modern optoelectronic devices [32,33]. The $YbYO_3$ doped ceramics are considered among the most promising host transparent materials for laser applications. Yb^{3+}: $(La_xY_{1-x})_2O_3$ nano-particles could be, in particular, a good gain medium for ytterbium high power pulse lasers as reported in [34,35].

The majority of scientific publications focused on the synthesis and characterization of oxides nano-crystals, their functional properties and possible applications in different fields. In this way, several chemical approaches have also been applied to obtain nano-crystals and control particle sizes and morphologies [36-41] Hydrothermal synthesis, for example, is often used due to its simplicity, allowing the control of particle shape and particle size distributions by making easy changes in the experimental conditions [42,43]. However, in wider experimental conditions, the co-precipitation method followed by a thermal treatment has also been successfully used for the fabrication and modification of nano-sized oxides [44,45].

In the present paper, therefore, two kinds of pure nano-powders $Gd_{0.745}Y_{1.255}O_3$ and $Yb_{1.4}Y_{0.6}O_3$ of mixed rare-earth-yttrium sesqui-oxides (diluted magnetics [46,47]) were successfully synthesized using the co-precipitation method. These mixed oxides nano-powders have been synthesized by capping its hydroxides to form precipitates and maintain the pH value. Addedly, the influence of the thermal treatment on particle sizes, crystallinity, morphological behaviour and optical properties was also investigated. This method offered advantages of simplicity and efficiency.

In general, any mixed oxide of yttrium with other rare earth element corresponding to formula $Y_{2-x}RE_xO_3$ [46], the rare earth element is used as a dopant in combination with yttrium oxide Y_2O_3 which has been considered as one of the most promising compounds for many applications such as optical amplifiers [48,49], cathode ray tubes (CRT), plasma display panels (PDP), high-temperature protective coatings, and it is also used in the manufacture of colored fluorescent lamps (yttrium oxide is a red emitting material under UV) [50-52]. The ability to give its particular physical properties (like luminescent properties) to rare earth elements and its high crystallographic stability, the yttrium oxide has been used as a host material.

Furthermore, the mixed rare earth-yttrium oxides $Y_{2-x}RE_xO_3$ are an important group of diluted magnetic semiconductors [46,47], especially when prepared in a nano-structured form. Particularly, the ytterbium–yttrium mixed oxides $Y_{2-x}Yb_xO_3$ are potential emitter materials for thermo-photovoltaic energy converters [53] and also promising ceramic lasers [54-56] due to the effect of Yb^{3+} ions (Yb^{3+} is a very attractive rare earth ion in the lanthanide series with unfilled f shells). On the other hand, the gadolinium-yttrium mixed oxides $Y_{2-x}Gd_xO_3$ (x = 0.10, 0.18, 0.41, 0.74 and 1.26) are also a special class of semi-magnetics semiconductors. The magnetic properties of all of them were studied in [47].

MATERIALS AND METHODS

Following a typical synthesis procedure for the preparation of $La_{1-x}Ca_xAlO_3 (0 \le x \le 0.6)$ nano-powders presented by Malika Diafi [57], a co-precipitation method was adopted to prepare $Gd_{0.745}Y_{1.255}O_3$ and $Yb_{1.4}Y_{0.6}O_3$ nano-powders following the same steps. First, all chemical reagents were used without any further purification. 0.014 mol of $Gd(NO_3)_3.6H_2O$ and 0.016 mol of $Y(NO_3)_3.6H_2O$ were dissolved separately in 25 ml of distilled water to form transparent solutions after that they were mixed. Under magnetic stirring, NaOH solution (12N) was slowly added drop by drop to the mixture to adjust

pH values and obtain a precipitate. The precipitate was filtered, washed with distilled water several times and dried at 90°C for 24h. Finally, the product obtained was calcined at different temperatures 600 °C, 800 °C and 1000°C in a tube oven for 4 h to form nano-powders.

Following the same steps and using $Yb(NO_3)_3.5H_2O$ precursor (0.014 mol), $Yb_{1.4}Y_{0.6}O_3$ nano-powder was also synthesized.

Powder X-ray diffraction analysis (XRD) of $Gd_{0.745}Y_{1.255}O_3$ and $Yb_{1.4}Y_{0.6}O_3$ was carried out at room temperature on a Philips PW 3830 diffractometer employing Co Kα (λ = 1.7889 Å) radiation with 0.016 steps. Peak positions and full width at half maximum (FWHM) were determined in the range (2θ) 15–75° to the recorded data, using the peak fitting module of the Origin program.

In addition, SEM images of the products were obtained using a scanning electron microscope (Tescan VEGA3 model), and the mean particle size was determined by Scherrer's formula [58]:

$$D = K\lambda/\beta\cos\theta \quad (1)$$

Where θ is the Bragg's angle of X-ray diffraction, λ is the wavelength of X-ray (1.7889 Å). K is a shape factor taken as 0.9, and β is full width at half maximum (FWHM).

The different nano-powders of our compounds calcined at 600, 800, and 1000°C were dispersed in distilled water with concentration (0.2g/l) to form suspension solutions, which were then utilized for the measurement of optical properties of absorption by an ultraviolet-visible spectrophotometer with optima SP-3000nano using quartz cells. All UV-Vis spectra were registered in the wavelength range from 200 nm to 500 nm at room temperature.

RESULTS AND DISCUSSION

XRD patterns of $Gd_{0.745}Y_{1.255}O_3$ and $Yb_{1.4}Y_{0.6}O_3$ nano-powders synthesized via Co-precipitation method and calcined at different temperatures (600 °C, 800 °C and 1000°C) are shown in Fig. 1 and Fig. 2, respectively.

Without calcination, XRD patterns of $Gd_{0.745}Y_{1.255}O_3$ and $Yb_{1.4}Y_{0.6}O_3$ show amorphous phases. Contrarily, both $Gd_{0.745}Y_{1.255}O_3$ and $Yb_{1.4}Y_{0.6}O_3$ powders which were calcined at 600, 800 and 1000 °C for 4 h can be indexed as pure-phases that are in good agreement with the data of ICSD Card No.73659 [46] and ICSD Card No. 84136

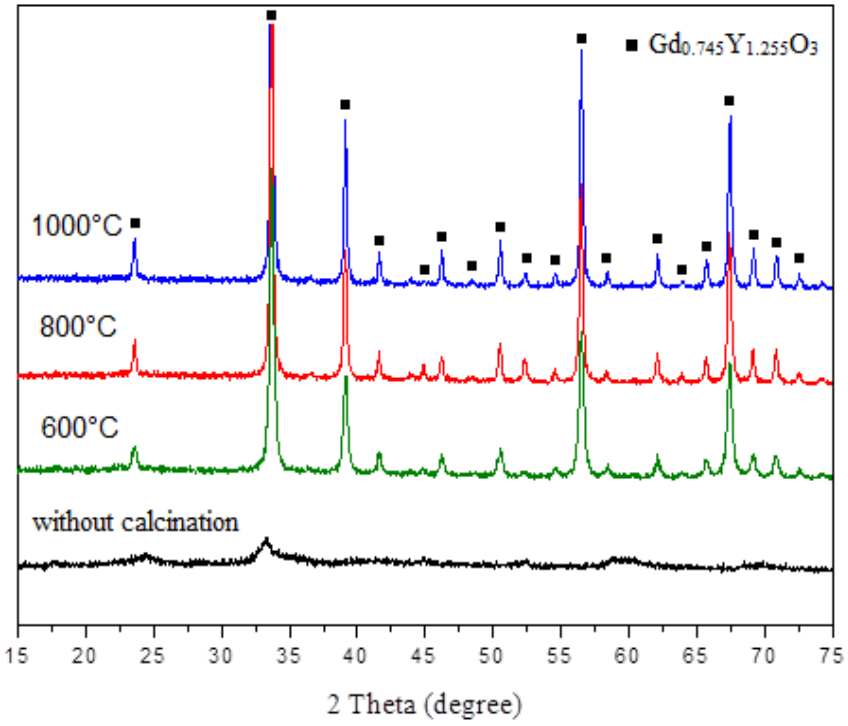

Fig. 1. XRD patterns of $Gd_{0.745}Y_{1.255}O_3$ nano-powders calcined for 4 h at various temperatures.

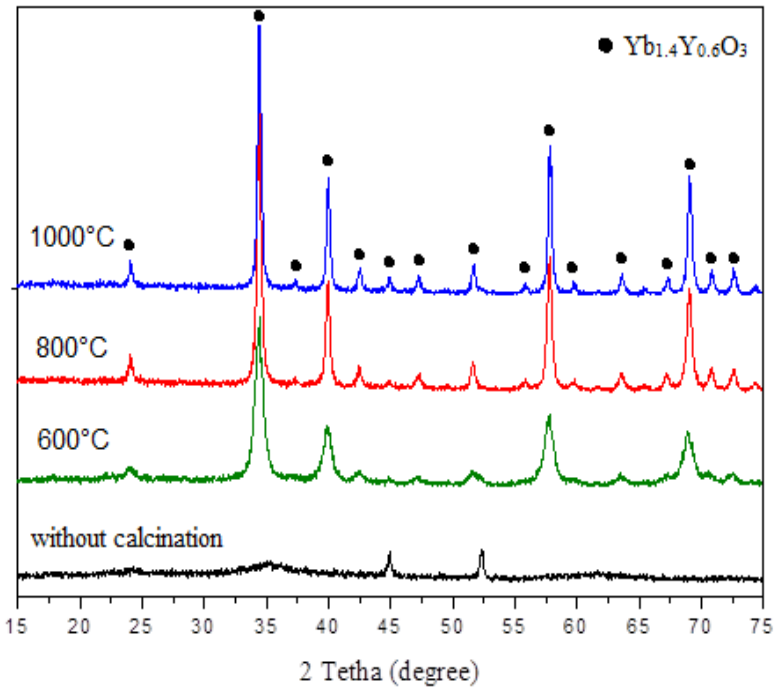

Fig. 2. XRD patterns of $Yb_{1.4}Y_{0.6}O_3$ nano-powders calcined for 4 h at various temperatures.

[47] belonging to the space group I a -3 (parameter a = 10.703Å and a = 10.4807Å), respectively.

In these experiments, the mixed oxides $Gd_{0.745}Y_{1.255}O_3$ and $Yb_{1.4}Y_{0.6}O_3$ were synthesized coincidentally instead of $GdYO_3$ and $YbYO_3$. It's worth noting that with the co-precipitation method $Gd_{0.745}Y_{1.255}O_3$ and $Yb_{1.4}Y_{0.6}O_3$ nano-powders could be synthesized using NaOH solution as a precipitate agent to form the hydroxide precipitations (amorphous phases):

$Gd(NO_3)_3 + Y(NO_3)_3 + 6OH^- \rightarrow Gd(OH)_3 + Y(OH)_3 + 6NO_3^-$ (this work) (2)

$Yb(NO_3)_3 + Y(NO_3)_3 + 6OH^- \rightarrow Yb(OH)3 + Y(OH)_3 + 6NO_3^-$ (this work) (3)

In this work, NaOH solution was added drop by drop to the mixture to adjust pH values to pH ≤ 9.5 to avoid the formation of $[Gd(OH)_6]^{3-}$, $[Yb(OH)_6]^{3-}$ and $[Y(OH)_6]^{3-}$ ions before the precipitation of $Gd(OH)_3$, $Yb(OH)_3$ and $Y(OH)_3$.

Zeheng Yang et al. [59], discussed the controlling molar ratio of NaOH in the synthesis of CuO nanoribbons. They proved experimentally that the molar ratio of NaOH to $Cu(NO_3)_2$ is an important parameter and that at high concentration of NaOH aqueous solutions, the hydroxide ions are first formed.

Moreover, Zhiwu Chen et al. in [60] reported that in the synthesis of bismuth ferrite powders, if ethanol is added to water, the surface tension of the solvent decreases and the hydroxide

Table 1. Average crystallite sizes of synthesized $Gd_{0.745}Y_{1.255}O_3$ and $Yb_{1.4}Y_{0.6}O_3$ nano-powders at different calcination temperatures.

	$Gd_{0.745}Y_{1.255}O_3$	$Yb_{1.4}Y_{0.6}O_3$
Thermal treatment temperatures (°C)	Average crystallite sizes (nm)	Average crystallite sizes (nm)
600	41.94	12.69
800	76.18	34.53
1000	99.60	50.12

precipitations form more quickly and thus have better dispersibility and are more easily dehydrated to form the powders.

In the thermal treatment (calcination) at various temperatures, Fig. 1 shows characteristic peaks of pure $Gd_{0.745}Y_{1.255}O_3$ single crystallographic structure. It can be seen that the XRD patterns of nano-powders at 600°C, 800°C and 1000°C were almost the same, which suggests that the crystallization of $Gd_{0.745}Y_{1.255}O_3$ structure could be at temperature under 600°C. In the case of $Yb_{1.4}Y_{0.6}O_3$ (Fig. 2), XRD patterns of nano-powders at 600°C, 800°C and 1000°C are also identical. Specially, two peaks in 2θ = 44.99° and 52.42° for $Yb_{1.4}Y_{0.6}O_3$ structure are clearly observed in the XRD pattern without calcination. Therefore, it can be confirmed that this is the first crystallization of the $Yb_{1.4}Y_{0.6}O_3$ phase.

It is evident that the width of the diffraction peaks of all precedent nano-powders indicates that the crystallite sizes are very small. As shown in Table 1, the average crystallite sizes calculated using the Debye-Scherrer formula for the $Gd_{0.745}Y_{1.255}O_3$ and $Yb_{1.4}Y_{0.6}O_3$ prepared samples increased as thermal treatment temperatures and crystallinity increased. This observation is in good agreement with literature [61-64]. In [61], Juliana B. Silva et al. stated that "the increase in peak intensities with temperature is due to the increase in crystallinity and particle size during the calcination process".

A similar behavior is in fact found for $Gd_{0.745}Y_{1.255}O_3$ and $Yb_{1.4}Y_{0.6}O_3$. From Fig. 3, in the case of $Gd_{0.745}Y_{1.255}O_3$ and around 2θ = 33.69°, the peak intensities increased with the temperatures of thermal treatment and crystallinity, which was also in accordance with the obtained values for crystallite size (increased from 38 nm to 78 nm).

There are many factors that influence the quality of the $Gd_{0.745}Y_{1.255}O_3$ and $Yb_{1.4}Y_{0.6}O_3$ ceramic nano-powders, such as powder agglomeration level, the temperature and the calcination time and especially the final particle size. According to the SEM images of prepared samples ($Gd_{0.745}Y_{1.255}O_3$ and $Yb_{1.4}Y_{0.6}O_3$) with thermal treatment, which are shown comparatively in Fig. 4, the nano-crystallites were not clearly visible in these images due to the SEMs resolution limit as well as the agglomeration of nano-powders.

However, a higher temperature motivated the grain growth as shown in image (D) (see Fig. 4). N. M. Al-Hada et al. [64] suggested that "as the temperature increases, several neighboring particles cling to each other, enlarging the particle size by melting their surfaces at higher temperature". This proposal has been previously discussed in literature [65,66].

UV–Vis absorption spectra of calcined

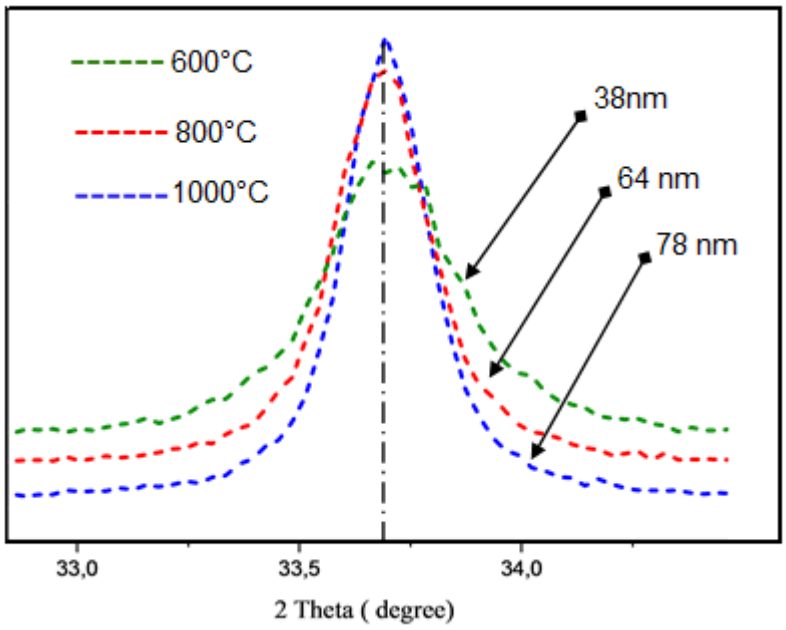

Fig. 3. Normalized XRD patterns of the peak reflection at 2θ=33.69° of $Gd_{0.745}Y_{1.255}O_3$ nano-powder calcined at different temperatures (2θ range from 33° to 34.5°).

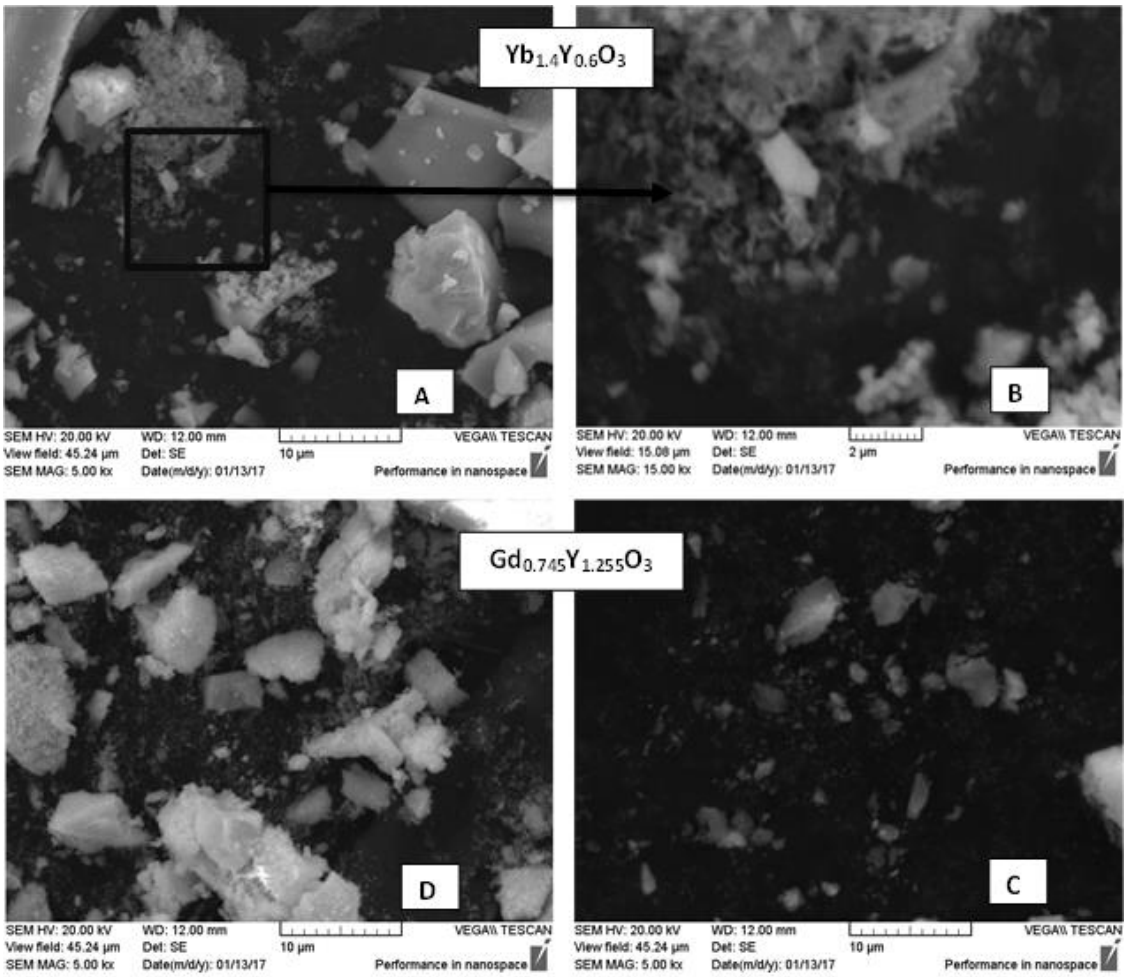

Fig. 4. SEM micrographs of $Gd_{0.745}Y_{1.255}O_3$ and $Yb_{1.4}Y_{0.6}O_3$ nano-powders calcined (A), (B), (C) at 600°C and (D) at 800°C.

$Gd_{0.745}Y_{1.255}O_3$ and $Yb_{1.4}Y_{0.6}O_3$ nano-powders are shown in Fig. 5 (a) and 6 (a), respectively. For all samples, as is observed clearly in UV spectra, strong absorption bands were detected at low wavelengths which corresponding to the band-to-band transition of the different phases. The obtained values of exciton energy E_{ex}, shown in Table 2, were calculated using the equation:

$$E_{ex} = hc/\lambda_{abs} \quad (4)$$

Where, h is Planck's constant, c the speed of light, and λ_{abs} is the wavelength of the absorption (nm).

On the other hand, it should be also noted that the absorbance decreases with the increasing wavelength, as reported in [67], this indicates the presence of an optical band-gap. The optical band-gap of $Gd_{0.745}Y_{1.255}O_3$ and $Yb_{1.4}Y_{0.6}O_3$ nano-powders were obtained using the Tauc plot method [68] as presented in Fig. 5 (b-d) and Fig 6 (b-d), respectively. The Tauc plot method based on the graph of $(\alpha h\nu)^2$ as a function of energy hν (eV), where α is the absorption coefficient and ν is the frequency.

For the $Yb_{1.4}Y_{0.6}O_3$, the values of the band-gap energy for the calcined nano-powders decrease with the temperature of calcination (from 4.22 to 3.95 eV) and consequently, with the increase in the particle size. These results are in good agreement with those reported for TiO_2 nanoparticles by S. Sharma et al. in [67], who added that: "Smaller crystallite size will have a larger band-gap and larger crystallite size will have a smaller band-gap".

In contrast, for $Gd_{0.745}Y_{1.255}O_3$, it can be seen that isn't the same behavior. The value of Eg was calculated to be ~3.61, ~ 3.82, and ~3.80 eV for the samples calcined at 600, 800, and

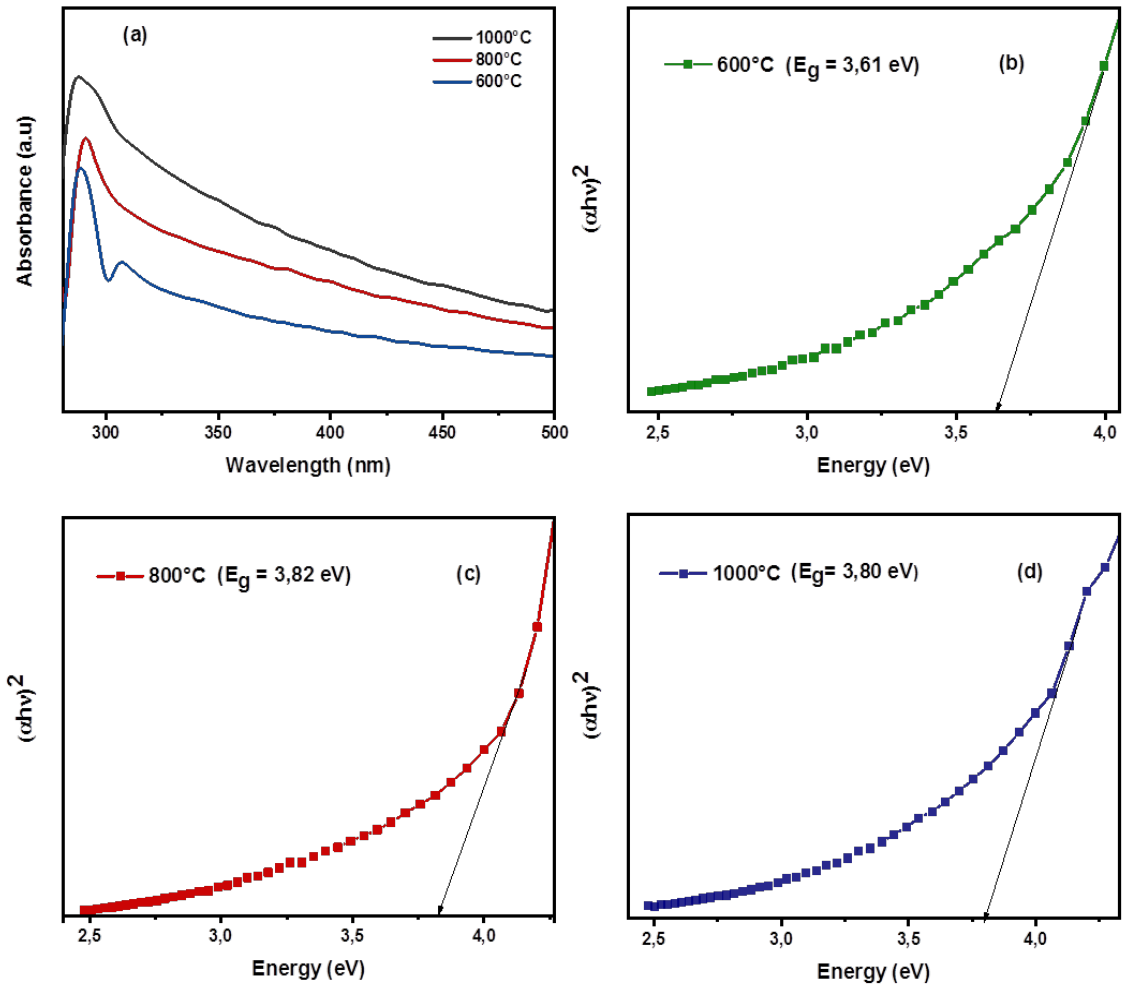

Fig. 5. (a) UV-Vis absorption spectra and (b-d) Tauc plots (to determine the energy band-gap) of calcined $Gd_{0.745}Y_{1.255}O_3$ nano-powders.

1000°C, respectively. Actually, the larger band-gap was observed for the nano-powder calcined at 800°C. This comportment may be attributed to the decreasing content of gadolinium in the mixed oxide phases, comparison to the Ytterbium content.

From these results and as a comparison, it should be noted that the Eg values of different nano-powders for $Yb_{1.4}Y_{0.6}O_3$ (with smaller particle sizes) are larger than those for $Gd_{0.745}Y_{1.255}O_3$. In the case of yttrium oxide nanoparticles, and based on photoluminescence and UV–vis results as is presented in [69], the influence of the particle size on the optical properties was also confirmed.

Table 2. Exciton energy (E_{ex}) of $Gd_{0.745}Y_{1.255}O_3$ and $Yb_{1.4}Y_{0.6}O_3$.

	$Gd_{0.745}Y_{1.255}O_3$	$Yb_{1.4}Y_{0.6}O_3$
sample	E_{ex}(eV)	E_{ex}(eV)
600	4.29	4.25
800	4.26	4.39
1000	4.31	4.40

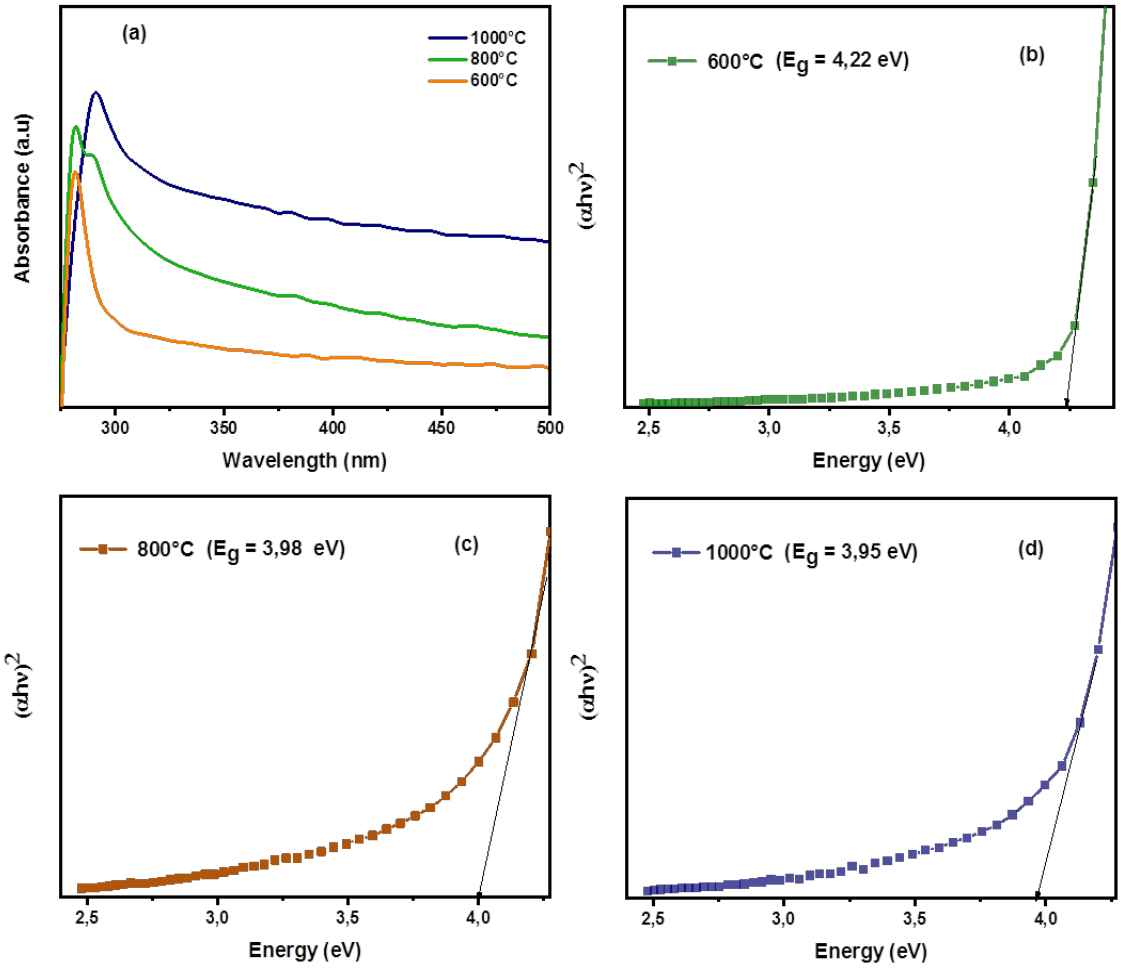

Fig. 6. (a) UV-Vis absorption spectra and (b-d) Tauc plots (to determine the energy band-gap) of calcined $Yb_{1.4}Y_{0.6}O_3$ nano-powders.

CONCLUSIONS

In this paper, pure $Gd_{0.745}Y_{1.255}O_3$ and $Yb_{1.4}Y_{0.6}O_3$ nano-powders of mixed rare-earth-yttrium sesquioxides (diluted magnetics) were successfully synthesized using the co-precipitation method with thermal treatment (calcination). The nano-powders were characterized by X-ray powder diffraction; their morphologies were analyzed by scanning electron microscope, their average sizes were calculated using the Scherrer formula, and their optical properties were studied using UV-Vis measurements and a Tauc plot calculation. We confirmed the good crystallinity of the $Gd_{0.745}Y_{1.255}O_3$ and $Yb_{1.4}Y_{0.6}O_3$ pure phases at different temperatures of thermal treatment (600°C, 800°C and 1000°C) and nano-metric particle sizes.

Under various pH values, the experiments were carried out to reveal the role of pH on the "co-precipitation" synthesis of $Gd_{0.745}Y_{1.255}O_3$ and $Yb_{1.4}Y_{0.6}O_3$ nano-powders. The pH values were adjusted by adding NaOH which, as a complexing agent, has a key role in the precipitation process.

The X-ray diffraction and the particle-size distribution demonstrated that, at different calcination temperatures 600°C, 800°C and 1000°C, particle size and cristallinity increased slightly as the annealing temperature increased. They were found to increase from ~ 42 nm at 600 °C to ~ 100 nm at 1000 °C for $Gd_{0.745}Y_{1.255}O_3$ and from ~ 13 nm at 600°C to ~ 50 nm at 1000°C for $Yb_{1.4}Y_{0.6}O_3$ which proved that higher temperatures motivated the grain growth. SEM analyses have also confirmed the growth and agglomeration of $Gd_{0.745}Y_{1.255}O_3$ and $Yb_{1.4}Y_{0.6}O_3$ nano-powders.

On the other hand, the band-gap of $Yb_{1.4}Y_{0.6}O_3$ nano-powders were found to be decreasing from 4.22 to 3.95 eV when the particle sizes increasing, but for $Gd_{0.745}Y_{1.255}O_3$ were found to be ~3.61, ~ 3.82, and ~3.80 eV for the samples calcined at

600, 800, and 1000°C, respectively. This confirmed the influence of the particle size on the optical properties.

From these results, it can be concluded that the formation of $Gd_{0.745}Y_{1.255}O_3$ and $Yb_{1.4}Y_{0.6}O_3$ nano-powders using a typical co-precipitation method has advantages of simplicity and efficiency, and also proves that thermal calcination is very effective for increasing cristallinity but with an increase in particle sizes which influence on the optical properties.

ACKNOWLEDGMENTS

The authors thank Pr. A. Guibadj for his helpful suggestions and support during the experiments.

CONFLICT OF INTEREST

The authors declare that there are no conflicts of interest regarding this article.

REFERENCES

1. Narang SB, Bahel S. Low loss dielectric ceramics for microwave applications : a review. Journal of Ceramic Processing Research. 2010; 11(3): p. 316-321.
2. Guo Z, Shao J, Lin H, Jiang M, Chen S, Li Z. Electrical conductivity & temperature sensitivity of ceramics based on NiO simple oxides for NTC applications. Journal of Materials Science: Materials in Electronics. 2017;28(16):11871-7.
3. Wang G, Zhang H, Sun X, Liu Y, Li Z. Characterization of a new system of NTC temperature-sensitive ceramics based on Al/F modified NiO simple oxides. Journal of Materials Science: Materials in Electronics. 2016;28(1):363-70.
4. Yang B, Zhang H, Guo J, Liu Y, Li Z. Electrical properties and thermal sensitivity of Ti/Y modified CuO-based ceramic thermistors. Frontiers of Materials Science. 2016;10(4):413-21.
5. Karaki T, Yan K, Miyamoto T, Adachi M. Lead-Free Piezoelectric Ceramics with Large Dielectric and Piezoelectric Constants Manufactured from BaTiO3Nano-Powder. Japanese Journal of Applied Physics. 2007;46(No. 4):L97-L8.
6. Rödel J, Webber KG, Dittmer R, Jo W, Kimura M, Damjanovic D. Transferring lead-free piezoelectric ceramics into application. Journal of the European Ceramic Society. 2015;35(6):1659-81.
7. Aksel E, Jones JL. Advances in lead-free piezoelectric materials for sensors and actuators. Sensors (Basel). 2010;10(3):1935-54.
8. Yan Y, Cho K-H, Priya S. Templated Grain Growth of 001 -Textured 0.675Pb(Mg1/3Nb2/3)O3-0.325PbTiO3 Piezoelectric Ceramics for Magnetic Field Sensors. Journal of the American Ceramic Society. 2011;94(6):1784-93.
9. Zhong J, Wu C, Wang D, Shi Y, Zhu J, Chen Q. Properties of novel CaBi2Ta2O9-(Na0.5Bi0.5)Bi2Ta2O9 solid solution-based high Curie temperature piezoelectric ceramics. Journal of Alloys and Compounds. 2019;794:210-7.
10. Huang R, Zhao Y, Yan D. (K0.5Na0.5)NbO3 lead-free ceramics with improved piezoelectricity and field-induced strain. Ceramics International. 2019;45(1):1450-4.
11. Padmapriya G, Manikandan A, Krishnasamy V, Jaganathan SK, Antony SA. Enhanced Catalytic Activity and Magnetic Properties of Spinel Mn x Zn1−x Fe2O4 (0.0 ≤ x ≤ 1.0) Nano-Photocatalysts by Microwave Irradiation Route. Journal of Superconductivity and Novel Magnetism. 2016;29(8):2141-9.
12. Gholizadeh A. La1− x Ca x Co1− y Mg y O3 nano-perovskites as CO oxidation catalysts: Structural and catalytic properties. Journal of the American Ceramic Society. 2016;100(3):859-66.
13. Remya GR, Solomon S, Thomas JK, John A. Optical and Dielectric Properties of Nano GdAlO3. Materials Today: Proceedings. 2015;2(3):1012-6.
14. Kumar S, Dwivedi GD, Joshi AG, Chatterjee S, Ghosh AK. Study of structural, dielectric, optical properties and electronic structure of Cr-doped LaInO 3 perovskite nanoparticles. Materials Characterization. 2017;131:108-15.
15. Ghodsal SM, Bodade AB, Chaudhari GN. Structural and Electrical Properties of Sr-Substituted Perovskites Nano-Crystalline LaCrO3. Asian Journal of Science and Technology. 2019; 10(05): p. 9665-9668.
16. Wagner N, Seshadri R, Rondinelli JM. Property control from polyhedral connectivity in ABO3 oxides. Physical Review B. 2019;100(6).
17. Qi H, Zuo R, Li J-f, Li L. Critical roles of the rhombohedral-phase inducers in morphotropic NaNbO3-BaTiO3-ABO3 quasi-ternary lead-free piezoelectric ceramics. Journal of the European Ceramic Society. 2018;38(16):5341-7.
18. Liu Y, Liu B, Xiang H, Zhou Y, Nian H, Chen H, et al. Theoretical investigation of anisotropic mechanical and thermal properties of AB O3 (A =Sr, Ba; B =Ti, Zr, Hf) perovskites. Journal of the American Ceramic Society. 2018;101(8):3527-40.
19. Vlazan P, Stoia M, Svera P, Poienar M, Sfirloaga P. Influence of Synthesis Method on the Morphology and Properties of ABO3 Materials. IOP Conference Series: Materials Science and Engineering. 2018;416:012076.
20. Reddy VN, Babu Naidu KC, Subba Rao T. Structural, Optical and Ferroelectric Properties of BaTiO3 Ceramics. Journal of Ovonic Research. 2016; 12(4): p. 185-191.
21. Danilov N, Vdovin G, Reznitskikh O, Medvedev D, Demin A, Tsiakaras P. Physico-chemical characterization and transport features of proton-conducting Sr-doped LaYO3 electrolyte ceramics. Journal of the European Ceramic Society. 2016;36(11):2795-800.
22. Okuyama Y, Kozai T, Sakai T, Matsuka M, Matsumoto H. Proton transport properties of La0.9M0.1YbO3−δ (M=Ba, Sr, Ca, Mg). Electrochimica Acta. 2013;95:54-9.
23. Lee JG, Hwang J, Hwang HJ, Jeon OS, Jang J, Kwon O, et al. A New Family of Perovskite Catalysts for Oxygen-Evolution Reaction in Alkaline Media: BaNiO3 and BaNi0.83O2.5. Journal of the American Chemical Society. 2016;138(10):3541-7.
24. Hwang J, Rao RR, Giordano L, Katayama Y, Yu Y, Shao-Horn Y. Perovskites in catalysis and electrocatalysis. Science. 2017;358(6364):751-6.
25. Zhu H, Zhang P, Dai S. Recent Advances of Lanthanum-Based Perovskite Oxides for Catalysis. ACS Catalysis. 2015;5(11):6370-85.
26. Xu X, Zhong Y, Shao Z. Double Perovskites in Catalysis, Electrocatalysis, and Photo(electro)catalysis. Trends in Chemistry. 2019;1(4):410-24.
27. Guldal NO, Figen HE, Baykara SZ. Perovskite catalysts for hydrogen production from hydrogen sulfide. International

Journal of Hydrogen Energy. 2018;43(2):1038-46.
28. Simmance K, Thompsett D, Wang W, Thiebaut B. Evaluation of perovskite catalysts prepared by flame spray pyrolysis for three-way catalyst activity under simulated gasoline exhaust feeds. Catalysis Today. 2019;320:40-50.
29. Sakai T, Isa K, Matsuka M, Kozai T, Okuyama Y, Ishihara T, et al. Electrochemical hydrogen pumps using Ba doped LaYbO3 type proton conducting electrolyte. International Journal of Hydrogen Energy. 2013;38(16):6842-7.
30. Song J, Kang J, Tan X, Meng B, Liu S. Proton conducting perovskite hollow fibre membranes with surface catalytic modification for enhanced hydrogen separation. Journal of the European Ceramic Society. 2016;36(7):1669-77.
31. Tamrakar RK, Upadhyay K, Bisen DP. Gamma ray induced thermoluminescence studies of yttrium (III) oxide nanopowders doped with gadolinium. Journal of Radiation Research and Applied Sciences. 2014;7(4):526-31.
32. Schmechel R, Kennedy M, von Seggern H, Winkler H, Kolbe M, Fischer RA, et al. Luminescence properties of nanocrystalline Y[sub 2]O[sub 3]:Eu[sup 3+] in different host materials. Journal of Applied Physics. 2001;89(3):1679.
33. Liu H, Zhai X, Wang L, Xiao S, Zhou J. Laser-induced spectra change in nanocrystalline GdYO3:Eu3+. Journal of Luminescence. 2015;165:85-7.
34. Lu J, Takaichi K, Uematsu T, Shirakawa A, Musha M, Ueda K-i, et al. Yb3+:Y2O3 Ceramics -- a Novel Solid-State Laser Material. Japanese Journal of Applied Physics. 2002;41(Part 2, No. 12A):L1373-L5.
35. Ivanov M, Kopylov Y, Kravchenko V, Li J, Medvedev A, Pan Y. Highly transparent ytterbium doped yttrium lanthanum oxide ceramics. Journal of Rare Earths. 2014;32(3):254-8.
36. Kumar E, Selvarajan P, Muthuraj D. Synthesis and characterization of CeO2 nanocrystals by solvothermal route. Materials Research. 2013;16(2):269-76.
37. Zhang Y, Wang M, Le Z, Huang G, Zou L, Chen Z. Preparation and characterization of pyrochlore oxide Y2Ti2O7 nanocrystals via gel-combustion route. Ceramics International. 2014;40(4):5223-30.
38. Zinatloo-Ajabshir S, Salavati-Niasari M, Hamadanian M. Preparation of nanocrystalline praseodymium oxide with different shapes via a simple thermal decomposition route. Journal of Materials Science: Materials in Electronics. 2015;27(1):998-1006.
39. Sanjabi S, Obeydavi A. Synthesis and characterization of nanocrystalline MgAl2O4 spinel via modified sol–gel method. Journal of Alloys and Compounds. 2015;645:535-40.
40. Yoko A, Seong G, Tomai T, Adschiri T. Continuous Flow Synthesis of Nanoparticles Using Supercritical Water: Process Design, Surface Control, and Nanohybrid Materials. KONA Powder and Particle Journal. 2020;37(0):28-41.
41. Lombardi J, Yang L, Pearsall FA, Farahmand N, Gai Z, Billinge SJL, et al. Stoichiometric Control over Ferroic Behavior in Ba(Ti1–xFex)O3 Nanocrystals. Chemistry of Materials. 2019;31(4):1318-35.
42. Biasotto G, Simões A, Foschini C, Antônio S, Zaghete M, Varela J. A novel synthesis of perovskite bismuth ferrite nanoparticles. Processing and Application of Ceramics. 2011;5(3):171-9.
43. Kaya İC, Kalem V, Akyildiz H. Hydrothermal synthesis of pseudocubic BaTiO 3 nanoparticles using TiO 2 nanofibers: Study on photocatalytic and dielectric properties. International Journal of Applied Ceramic Technology. 2019;16(4):1557-69.
44. Mardani R. The synthesis of Ba2+-doped multiferroic BiFeO3 nanoparticles using co-precipitation method in the presence of various surfactants and the investigation of structural and magnetic features. Modern Physics Letters B. 2017;31(15):1750169.
45. Haron W, Wisitsoraat A, Sirimahachai U, Wongnawa S. A simple synthesis and characterization of LaMO3 (M= Al, Co, Fe, Gd) perovskite via chemical co-precipitation method. Songklanakarin Journal of Science & Technology. 2018; 40(3): p. 484-491.
46. Mitric M, Onnerud P, Rodic D, Tellgren R, Szytula A, Napijalo ML. The preferential site occupation and magnetic properties of GdxY2−xO3. Journal of Physics and Chemistry of Solids. 1993;54(8):967-72.
47. Mitric M, Antic B, Balanda M, Rodic D, Napijalo ML. An X-ray diffraction and magnetic susceptibility study of YbxY2-xO3. Journal of Physics: Condensed Matter. 1997; 9(20): p. 4103-4111.
48. Kouass S, Sahbani S, Dhaouadi H, Touati F. Chromium substitution induced effects on the structure optical and electrical properties of yttrium oxide. Journal of the Australian Ceramic Society. 2017;53(2):403-13.
49. Waite C, Mann R, Diaz AL. Measurement of host-to-activator transfer efficiency in nano-crystalline Y2O3:Eu3+ under VUV excitation. Journal of Solid State Chemistry. 2013;198:357-63.
50. Huang H, Nakamura M, Su P, Fasching R, Saito Y, Prinz FB. High-Performance Ultrathin Solid Oxide Fuel Cells for Low-Temperature Operation. Journal of The Electrochemical Society. 2007;154(1):B20.
51. Guo B, Yim H, Hwang W, Nowell M, Luo Z. Crystalline phase of Y2O3:Eu particles generated in a substrate-free flame process. Particuology. 2011;9(1):24-31.
52. Cannas C, Casu M, Mainas M, Musinu A, Piccaluga G, Polizzi S, et al. Synthesis, characterisation and optical properties of nanocrystalline Y2O3–Eu3+dispersed in a silica matrix by a deposition–precipitation method. J Mater Chem. 2003;13(12):3079-84.
53. Panitz J-C. Characterization of ytterbium-yttrium mixed oxides using Raman spectroscopy and x-ray powder diffraction. Journal of Raman Spectroscopy. 1999;30(11):1035-42.
54. Mouzon J, Dujardin C, Tillement O, Odén M. Synthesis and optical properties of Yb0.6Y1.4O3 transparent ceramics. Journal of Alloys and Compounds. 2008;464(1-2):407-11.
55. Takaichi K, Yagi H, Lu J, Bisson J-F, Shirakawa A, Ueda K-i, et al. Highly efficient continuous-wave operation at 1030 and 1075 nm wavelengths of LD-pumped Yb3+:Y2O3 ceramic lasers. Applied Physics Letters. 2004;84(3):317-9.
56. Tel'nova GB, Konovalov AA, Shvorneva LI, Kutsev SV, Solntsev KA. Phase transformations during the synthesis and sintering of Y2 − x Yb x O3 nanopowders. Inorganic Materials. 2011;47(4):390-5.
57. Diafi M. Synthèse et propriétés physiques d'oxyde mixtes à base de lanthane calcium et aluminium. 2013. Doctoral dissertation, Universite Mohamed Khider-Biskra.
58. Yang Z, Xu J, Zhang W, Liu A, Tang S. Controlled synthesis of CuO nanostructures by a simple solution route. Journal of Solid State Chemistry. 2007;180(4):1390-6.
59. Klug HP, Alexander LE. X-Ray Diffraction Procedures: For Polycrystalline and Amorphous Materials. 2nd ed. New York-Sydney-Toronto: John Wiley & Sons; 1974.
60. Chen Z, Wu Y, Hu J. Ethanol-Assisted Hydrothermal Synthe-

sis and Characterization of BiFeO3 Nanopowders. Journal of the American Ceramic Society. 2013;96(5):1345-8.
61. Silva JB, Brito Wd, Mohallem NDS. Influence of heat treatment on cobalt ferrite ceramic powders. Materials Science and Engineering: B. 2004;112(2-3):182-7.
62. Krauser MdO, Oliveira HHdS, Cebim MA, Davolos MR. Relationship between scintillation properties and crystallite sizes in Y2O3:Eu3+. Journal of Luminescence. 2018;203:100-4.
63. Exner J, Schubert M, Hanft D, Kita J, Moos R. How to treat powders for the room temperature aerosol deposition method to avoid porous, low strength ceramic films. Journal of the European Ceramic Society. 2019;39(2-3):592-600.
64. Al-Hada NM, Halimah MK, Shaari AH, Saion E, Aziz SA, Mustafa IS. Structural and Morphological Properties of Manganese-Zinc Ferrite Nanoparticles Prepared by Thermal Treatment Route. Solid State Phenomena. 2019;290:307-13.
65. Kamari H, Al-Hada N, Saion E, Shaari A, Talib Z, Flaifel M, et al. Calcined Solution-Based PVP Influence on ZnO Semiconductor Nanoparticle Properties. Crystals. 2017;7(2):2.
66. Al-Hada NM, Saion EB, Shaari AH, Kamarudeen MA, Flaifel MH, Gene SA. Synthesis, Structural and Morphological Properties of Cadmium Oxide Nanoparticles Prepared by Thermal Treatment Method. Advanced Materials Research. 2015;1107:291-4.
67. Sharma S, Venkata Dhanunjaya Reddy A, Jayarambabu N, Vikram Manoj Kumar N, Saineetha A, Venkateswara Rao K, et al. Synthesis and characterization of Titanium dioxide nanopowder for various energy and environmental applications. Materials Today: Proceedings. 2020;26:158-61.
68. Tauc J, Grigorovici R, Vancu A. Optical Properties and Electronic Structure of Amorphous Germanium. physica status solidi (b). 1966;15(2):627-37.
69. Srinivasan R, Yogamalar R, Bose AC. Structural and optical studies of yttrium oxide nanoparticles synthesized by co-precipitation method. Materials Research Bulletin. 2010;45(9):1165-70.